Shape Memory Zirconia Foams Through Ice Templating

Xueying Zhao[a], Alan Lai[a], Christopher A. Schuh[a*]

[a]Department of Materials Science and Engineering, Massachusetts Institute of Technology (MIT), Cambridge, MA, USA.

[*]Corresponding author. Email: schuh@mit.edu

Abstract

Ceria doped zirconia has been shown to exhibit enhanced shape memory properties in small volume structures such as particles and micropillars. Here those properties are translated into macroscopic materials through the fabrication of zirconia foams by ice templating. Directional freezing is used to produce foams with micron-sized pores and struts that can locally take advantage of the shape memory effect due to their fine scale. The foams are subjected to thermal cycling and x-ray diffraction analysis to evaluate the martensitic transformation that underlies shape memory properties, and are found to survive the transformation through multiple cycles.

Graphical abstract
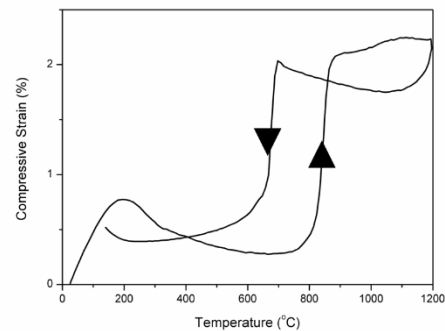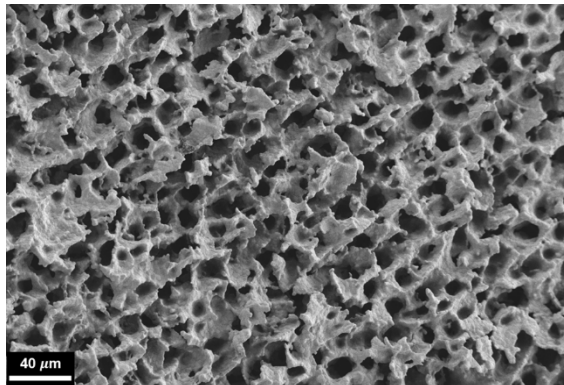
Keywords:
Freeze casting
Foams
Shape memory effect
Martensitic phase transformation

The shape memory effect in partially stabilized zirconia ceramics was discussed as early as three decades ago, but because zirconia is brittle and susceptible to cracking during the martensitic transformation, its shape memory behavior was limited to low strains and few cycles [1-3]. Recently, Lai et al. were able to alleviate the cracking problem in shape memory ceramics by producing oligocrystalline and single-crystalline structures in small volumes [4]. At the scale of a micron or so, zirconia pillars [5] and particles [6] exhibit improved shape memory properties compared with bulk zirconia,

namely much larger strains (up to ~8%) and the ability to cycle through the transformation many times (up to hundreds) without cracking. The origin of this size effect lies in the relief of constraint; the paucity of grain boundaries and prevalence of free surfaces lead to transformation stress accommodation rather than cracking.

It would be highly desirable to construct macroscale materials from such micro-scale structures, in order to translate the desirable shape memory properties of ceramics to applications with scales greater than the micrometer level. In related shape memory materials such as the copper-based [7] and magnetic [8] shape memory alloys, such scaling has been accomplished by a variety of approaches, including through the formation of long microfibers or open-cell foams [9]. The three dimensional geometry of a foam is attractive for large-scale forms, while their porosity admits a large area of free surfaces to accommodate the transformation stresses that would otherwise lead to cracking [10, 11]. Such approaches should be relevant to shape memory ceramics as well, and our purpose in this letter is to demonstrate the first shape memory ceramic material with bulk dimensions, produced as a foam. We specifically strive to produce foam struts that are oligocrystalline, each of which would function like a shape memory micro-pillar.

We employ the foam synthesis method of freeze casting, which has been applied to a wide range of materials to create porous structures, including alumina, silicon nitride, titanium, tungsten, hydroxyapatite, etc. [12-19]. A water suspension of the ceramic particles is frozen and ice is then sublimated under reduced pressure, creating porosity in place of the ice crystals; the resulting porous green body is sintered to consolidate the ceramic foam struts and walls [20].

We use ice templating with directional solidification, similar to the approach reported by Chino and Dunand [13]. The general set-up for such experiments is shown in Fig. 1a, and comprises a mold with low conductivity side walls matched with a high conductivity base, through which most of the heat is extracted and directional solidification thus effected. In the simplest case, one can cast with a fixed base temperature and no control over the solidification rate; we achieved this condition using glass side walls wrapped in cotton. In a more complex case, one can program a changing base temperature so as to manipulate the rate of cooling; we achieved this by varying the boundary condition of the cold plate (T_o) with a thermoelectric cooler attached to a copper casting base with a programmed input voltage, with low conductivity PTFE side walls.

Oxide powders were acquired from Sigma-Aldrich, and had the following particle sizes: ZrO_2, <100 nm; CeO_2, <50 nm. The powders were mixed with water to form a slurry with a solids loading of 12 vol%. An anionic dispersing agent (Darvan C-N, consisting of ammonium polymethacrylate and water) was added as 1 wt.% of the powder to improve the dispersion of ceramic powders in the solvent. Polyvinyl alcohol (PVA) was also added to serve as a binder to provide green strength after

sublimation of the ice and was added as 2 wt.% of the powder. After freeze casting the green body was sintered at 1500°C for 10 hours where interdiffusion of the oxides took place.

The solidification rate affects the microstructure of the foam that is produced, depending on its relation to the critical rate for particle ejection, and is dictated by the rate of heat extraction. An understanding of the heat transfer situation is therefore desirable to produce uniform foams, and here we use finite element modeling of the solidification process to help guide the foam synthesis. Since we model an axisymmetric situation with well-insulated side walls, the problem devolves to a one-dimensional problem of heat conduction along the z-axis, with the added complexity of the solidification front that releases the heat of fusion as it propagates. We solve this problem numerically using the ABAQUS 6.14-3 finite element solver, under the initial condition that the cast slurry is at room temperature: $T_i = 20$°C, and for simplicity we neglect details of the solid loading and simply model the solidification of ice from water (heat of fusion: 333.6 J/g, density of ice: 916.7 kg/m^3, density of water: 1000 kg/m^3, thermal conductivity of ice: 2.25 W/m·K, thermal conductivity of water: 0.58 W/m·K, specific heat of ice: 2030 J/kg·K, specific heat of water: 4187J/kg·K). A convective boundary condition with a coefficient of 5 W/m^{2}K to the ambient temperature of 20°C is applied to the top surface and the bottom surface is in contact with the cold plate at an assigned temperature T_o.

Two conditions are compared in this work:

A constant cold mold temperature $T_o = -10$°C. For this condition the finite element model closely matches the expected Neumann solution for a semi-infinite problem, at least at short times. The predicted ice front velocity shown in Fig. 1b is found to span a large range from hundreds of micrometers at the outset, to values more than an order of magnitude lower by the time the front has moved 5 mm. The problem with this wide range of velocities is that it spans the expected transition from particle engulfing to particle ejection. Fig. 1c shows a photograph of the foam structure produced by casting in this mode, which shows a clear two-zone solidification structure. There is a high density layer on the bottom, apparently due to the freezing that occurred there being too rapid for particle ejection [14]. After about 2.5 mm along the freezing direction, we observe a transition to a homogeneous porous regime. We associate this structural transition with the velocity of the ice front dropping below the critical particle ejection velocity. Comparing the location of the transition with the model results in Fig. 1b, we infer that the critical velocity is between about 20 and 30 μm/s. The reported critical velocity is about 2 μm/s for particles with diameter between 1 and 10 μm in silica-water slurry [21]. Since the critical velocity is inversely proportional to the particle radius, it is reasonable to see a value about an order of magnitude higher for our system where the particle diameter is about 100 nm [14].

A parabolic decrease in T_o with time was also explored as a means of avoiding the structural transition described above. In order to attenuate the rate of heat extraction in the early stages and so avoid the particle engulfing regime, we designed a temperature profile ranging from 0 to -10°C over 14 minutes, i.e., $T_o = -10\sqrt{t/14}$ (T_o in °C and t in min). This mold temperature profile yields a predicted ice front velocity as shown in Fig. 1b in red, which is nearly constant and on the order of 10 µm/s, below the transition velocity and in the range that produces uniform foam. Experimentally, we tuned the applied voltage to the Peltier cooling stage to attain nearly the same profile and indeed, the resulting foam appeared uniform along its length.
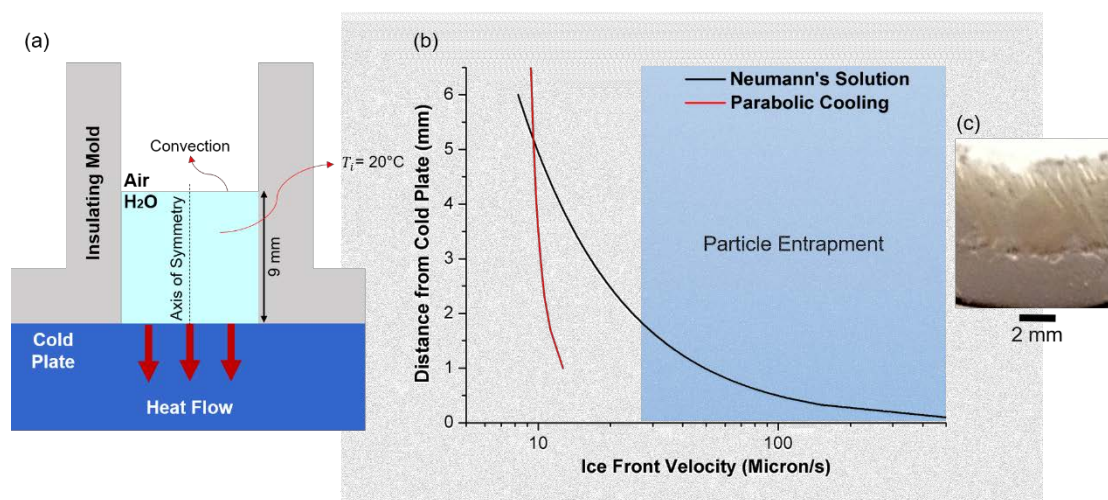

Fig. 1. (a) Schematic of directional freezing setup comprised of insulating side walls and conductive base (b) Predicted ice front velocities as a function of distance from the cold plate based on constant and changing boundary conditions (c) Sample chilled by constant cold temperature, showing a physical demarcation.

Foams produced under this controlled cooling regime had pore structures such as shown in Fig. 2a. With open pores of uniform size and struts on the order of microns that exhibit a high ratio of surface area to grain boundary area, these are oligocrystalline grain structures. The foam structure was quantified using micro computed x-ray tomography with an X-TEK XT H 225 ST instrument. Fig. 2b shows a 3D rendering of a typical foam structure, with its vertical and horizontal slices given in Figs. 2c and 2d respectively. The pore size distribution measured at various slices along the casting direction is shown in Fig. 2e. The average pore size (equivalent spherical diameter) is of order ~20 microns, while the median pore size is about 10 microns, and remains close to this value all the way through the sampled volume. This observation is supportive of the expected constant solidification velocity from Fig. 1b. It is also noteworthy that Fig. 2c shows both lamellar/dendritic and reticulated pores. The literature has reported the formation of lamellar structures through ice templating by exploiting the anisotropy in the interfacial energies of ice [14, 20]. The formation of reticulated pores, however, is attributed to the effect of PVA addition. This is consistent with the finding of Zuo et al. that PVA addition led to more open pores [22]."
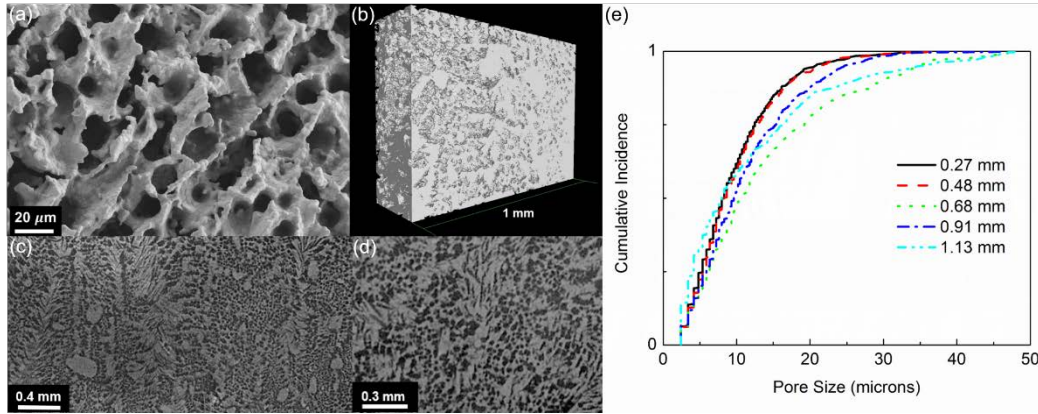
Fig. 2. (a) Transverse section (plane perpendicular to thermal gradient) of a foam subjected to parabolic cooling as viewed in a scanning electron microscope (b) 3D rendering of a typical foam structure (c) Longitudinal section (plane parallel to thermal gradient) (d) Transverse section (e) Pore size distribution at various distances from the cold plate.

The resulting foams had a relative density of about 0.34. With typical strut widths of 7.4 µm and grain sizes of 3.0 to 3.5 microns, these oligocrystalline structures are comparable to the dimensions reported in Ref. [23] in micropillar geometries to exhibit reproducible cyclic shape memory and superelasticity. This is explored in more detail in Fig. 3, where the thermally induced transformation is observed with differential scanning calorimetry (DSC) and thermomechanical analysis (TMA). In the DSC curve (Fig. 3a), the endothermic peak on heating corresponds to the transformation from monoclinic to tetragonal, or in the shape memory vernacular, martensite to austenite, respectively. The exothermic peak on cooling corresponds to the reverse transformation from tetragonal to monoclinic. The transformation temperatures measured from both techniques are in agreement: austenite start (A_s) is around 810℃; austenite finish (A_f) is around 868℃; martensite start (M_s) is around 728℃ and martensite finish (M_f) is around 642℃. At the composition of this foam (6 mol% ceria), the expected set of transformation temperatures based on linear interpolation from the literature [24] would be about 766℃, 793℃, 677℃, and 632℃ (austenite start temperature, peak temperature during heating, martensite start temperature and peak temperature during cooling, respectively); the agreement is very good.

The most important result from Fig. 3 is the recoverable shape change associated with the transformation under light stress bias. In the TMA experiment, the foam was held under a very small constant uniaxial compressive stress of 4.2 kPa during the thermal cycle. The results show that the foam experienced a large dimensional change of almost 2% (Fig. 3b). This is a high strain level compared with the shape memory strains that are attainable in bulk ceramics. For example, Tiefenbach [25] reported a thermally-activated strain below 1%, accompanied by cracking, in bulk 9 mol% ceria-doped zirconia.
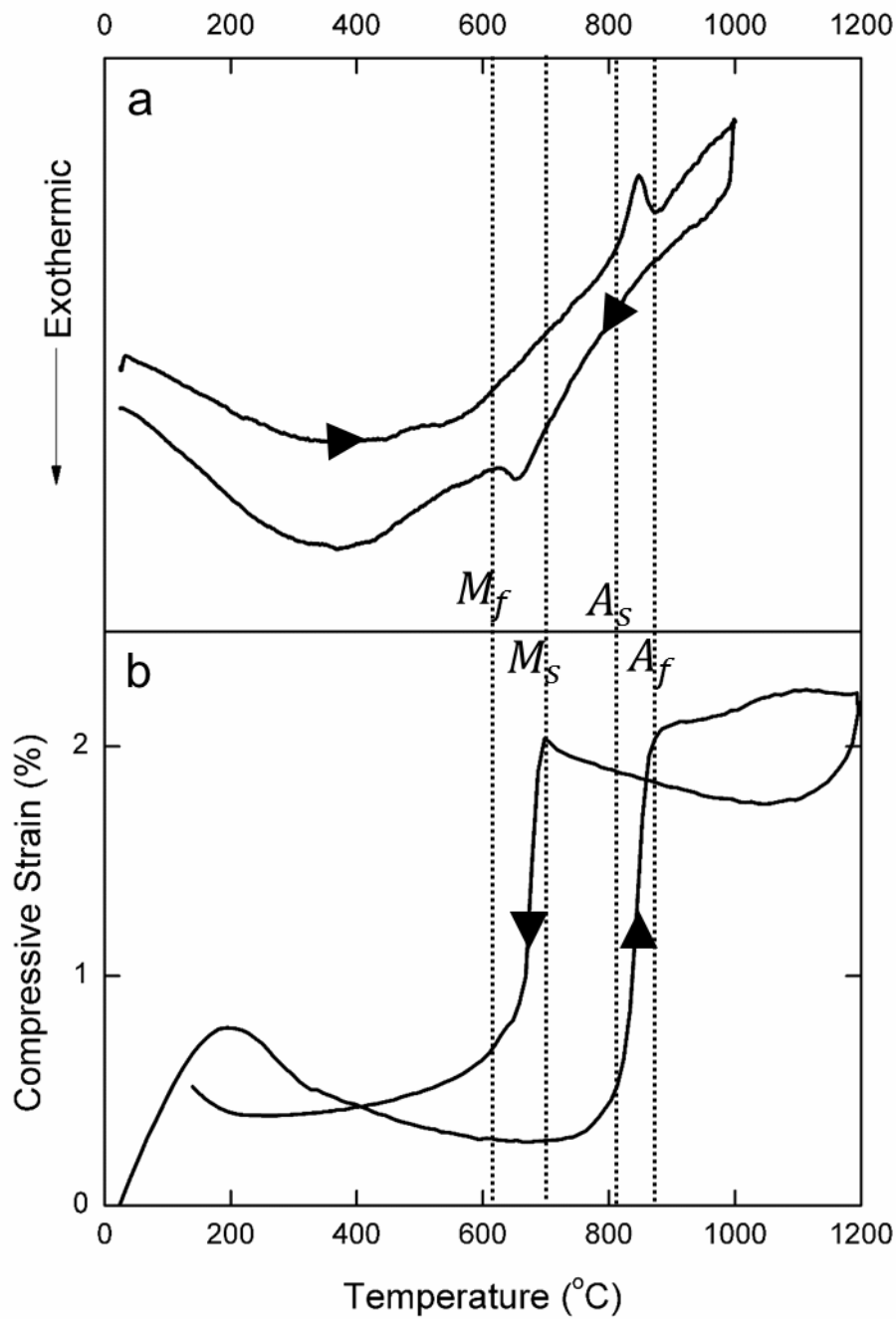
Fig. 3. DSC (a) and TMA (b) curves of 6 mol% ceria doped zirconia foam where transformation temperatures are in line with dimensional changes.

We next examine a foam of a different composition, 14.4 mol% ceria, which yields a martensite finish temperature M_f around room temperature, but an austenite start temperature at elevated temperatures. Thus, this sample should be able to convert to martensite upon loading but then remain in that phase upon unloading. This is a convenient condition, therefore, in which to directly verify stress-induced martensitic transformation in the foam. Foams are subjected to compression at room temperature

in an Instron 8848 Microtester and XRD studies are conducted with a PANalytical X'Pert Pro diffractometer using nickel filtered Cu K_α radiation in the 2θ range 20-90°. In the XRD patterns of Fig. 4, the tetragonal phase is quickly identified by inspecting the peak at 30.1° and the monoclinic phase has two characteristic peaks labeled at 28.1° and 31.2°. The as-produced foam was mostly comprised of the tetragonal phase with only 15% monoclinic phase before the application of any stress (Fig. 4a). Upon compression, the tetragonal phase transformed to the monoclinic phase: up to 22% monoclinic phase is measured at a stress of 1.2 MPa and 69% at 3.1 MPa of stress (Figs. 4b and c). This constitutes direct evidence of stress-induced transformation without fracture in these shape memory ceramic foams.
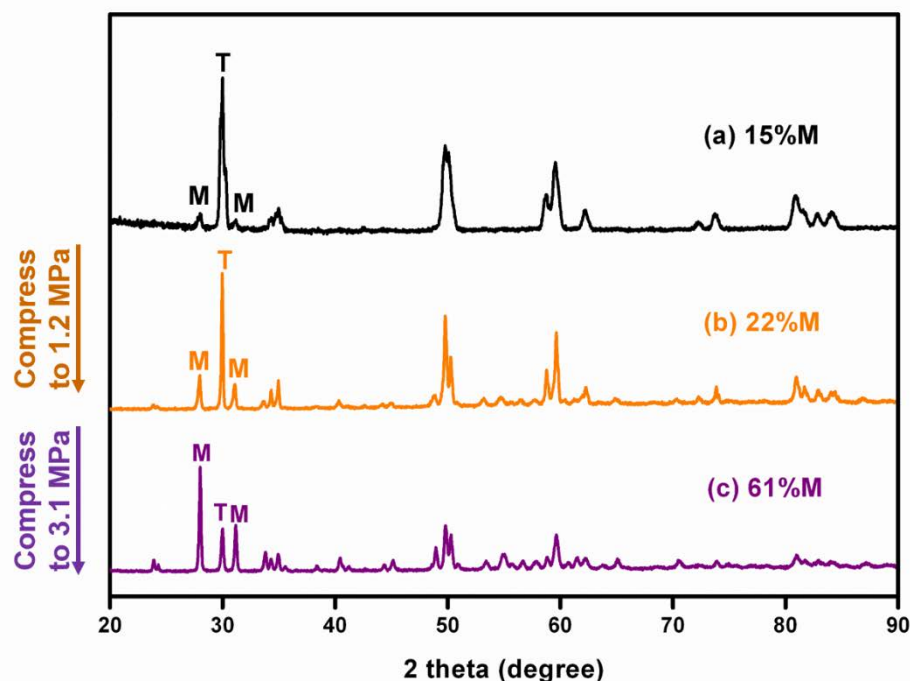

Fig. 4. XRD patterns of foam sample (a) before compression, (b) and (c) after compression showing stress induced transformation

To summarize, a first demonstration of the synthesis and validation of shape memory properties has been presented for zirconia ceramics. Directional freezing with a parabolic decrease in mold temperature over time led to a nominally constant solidification rate and produced a quantitatively uniform open-cell foam structure with oligocrystalline struts. The martensitic transformation has been observed both in stress-driven and thermally-driven modes, and the recoverable strain of almost 2% is a value much higher than achievable in monolithic zirconia.

finite element method and Mr. Aaron Johnson of Amphenol TCS, Nashua NH, for his help with tomography.

References

[1]   P. E. Reyes-Morel and I. W. Chen, "Transformation Plasticity of Ceo2-Stabilized Tetragonal Zirconia Polycrystals: I, Stress Assistance and Auto-Catalysis," *Journal of the American Ceramic Society,* vol. 71, pp. 343-353, May 1988.

[2]   P. E. Reyes-Morel, J. S. Cherng, and I. W. Chen, "Transformation Plasticity of Ceo2-Stabilized Tetragonal Zirconia Polycrystals: II, Pseudoelasticity and Shape Memory Effect," *Journal of the American Ceramic Society,* vol. 71, pp. 648-657, Aug 1988.

[3]   M. V. Swain, "Shape Memory Behavior in Partially-Stabilized Zirconia Ceramics," *Nature,* vol. 322, pp. 234-236, Jul 17 1986.

[4]   A. Lai, Z. H. Du, C. L. Gan, and C. A. Schuh, "Shape Memory and Superelastic Ceramics at Small Scales," *Science,* vol. 341, pp. 1505-1508, Sep 27 2013.

[5]   X. M. Zeng, Z. H. Du, C. A. Schuh, N. Tamura, and C. L. Gan, "Microstructure, crystallization and shape memory behavior of titania and yttria co-doped zirconia," *Journal of the European Ceramic Society,* vol. 36, pp. 1277-1283, Apr 2016.

[6]   Z. Du, X. M. Zeng, Q. Liu, C. A. Schuh, and C. L. Gan, "Superelasticity in micro-scale shape memory ceramic particles," *Acta Materialia,* vol. 123, pp. 255-263, 2017.

[7]   S. M. Ueland, Y. Chen, and C. A. Schuh, "Oligocrystalline Shape Memory Alloys," *Advanced Functional Materials,* vol. 22, pp. 2094-2099, May 23 2012.

[8]   Y. Boonyongmaneerat, M. Chmielus, D. C. Dunand, and P. Mullner, "Increasing magnetoplasticity in polycrystalline Ni-Mn-Ga by reducing internal constraints through porosity," *Physical Review Letters,* vol. 99, Dec 14 2007.

[9]   D. C. Dunand and P. Mullner, "Size Effects on Magnetic Actuation in Ni-Mn-Ga Shape-Memory Alloys," *Advanced Materials,* vol. 23, pp. 216-232, Jan 11 2011.

[10]   S. Arnaboldi, P. Bassani, F. Passaretti, A. Redaelli, and A. Tuissi, "Functional Characterization of Shape Memory CuZnAl Open-Cell Foams by Molten Metal Infiltration," *Journal of Materials Engineering and Performance,* vol. 20, pp. 544-550, Jul 2011.

[11]   M. Chmielus, X. X. Zhang, C. Witherspoon, D. C. Dunand, and P. Mullner, "Giant magnetic-field-induced strains in polycrystalline Ni-Mn-Ga foams," *Nature Materials,* vol. 8, pp. 863-866, Nov 2009.

[12]   R. Ahmad, J. H. Ha, and I. H. Song, "Synthesis of open-cell particle-stabilized Al2O3 foam using Al(OH)(3) particles," *Scripta Materialia,* vol. 76, pp. 85-88, Apr 2014.

[13]   Y. Chino and D. C. Dunand, "Directionally freeze-cast titanium foam with aligned, elongated pores," *Acta Materialia,* vol. 56, pp. 105-113, Jan 2008.

[14]   S. Deville, E. Saiz, and A. P. Tomsia, "Ice-templated porous alumina structures," *Acta Materialia,* vol. 55, pp. 1965-1974, Apr 2007.

[15]   T. Fukasawa, M. Ando, T. Ohji, and S. Kanzaki, "Synthesis of porous ceramics with complex pore structure by freeze-dry processing," *Journal of the American Ceramic Society,* vol. 84, pp. 230-232, Jan 2001.

[16]   T. Fukasawa, Z. Y. Deng, M. Ando, T. Ohji, and S. Kanzaki, "Synthesis of porous silicon nitride with unidirectionally aligned channels using freeze-drying process," *Journal of the American Ceramic Society,* vol. 85, pp. 2151-2155, Sep 2002.

[17]   A. Rothlisberger, S. Haberli, R. Spolenak, and D. C. Dunand, "Synthesis, structure and mechanical properties of ice-templated tungsten foams," *Journal of Materials Research,* vol. 31, pp. 753-764, Mar 28 2016.

[18]   B. H. Yoon, W. Y. Choi, H. E. Kim, J. H. Kim, and Y. H. Koh, "Aligned porous alumina ceramics with high compressive strengths for bone tissue engineering," *Scripta Materialia,* vol. 58, pp. 537-540, Apr 2008.

[19]   K. C. Zhou, Y. Zhang, D. Zhang, X. Y. Zhang, Z. Y. Li, G. Liu*, et al.*, "Porous hydroxyapatite ceramics fabricated by an ice-templating method," *Scripta Materialia,* vol. 64, pp. 426-429, Mar 2011.

[20]   S. Deville, "Freeze-casting of porous ceramics: A review of current achievements and issues," *Advanced Engineering Materials,* vol. 10, pp. 155-169, Mar 2008.

[21]   R. Asthana and S. N. Tewari, "The Engulfment of Foreign Particles by a Freezing Interface," *Journal of Materials Science,* vol. 28, pp. 5414-5425, Oct 15 1993.

[22]   K. H. Zuo, Y. P. Zeng, and D. L. Jiang, "Effect of polyvinyl alcohol additive on the pore structure and morphology of the freeze-cast hydroxyapatite ceramics," *Materials Science & Engineering C-Materials for Biological Applications,* vol. 30, pp. 283-287, Jan 30 2010.

[23]   Z. H. Du, X. M. Zeng, Q. Liu, A. Lai, S. Amini, A. Miserez*, et al.*, "Size effects and shape memory properties in ZrO2 ceramic micro- and nano-pillars," *Scripta Materialia,* vol. 101, pp. 40-43, May 2015.

[24]   M. Yashima, T. Mitsuhashi, H. Takashina, M. Kakihana, T. Ikegami, and M. Yoshimura, "Tetragonal-Monoclinic Phase-Transition Enthalpy and Temperature of Zro2-Ceo2 Solid-Solutions," *Journal of the American Ceramic Society,* vol. 78, pp. 2225-2228, Aug 1995.

[25]   A. Tiefenbach, S. Wagner, R. Oberacker, and B. Hoffmann, "Measurement of the t -> m and m -> t transformations in Ce-TZP by dilatometry and impedance spectroscopy," *Journal of the European Ceramic Society,* vol. 22, pp. 337-345, Mar 2002.